Defense Threat Reduction Agency
8725 John J. Kingman Road, MS 6201
Fort Belvoir, VA 22060-6201

DTRA-TR-05-30

TECHNICAL REPORT

A Study of Long-Range Seismic Profile Data in Western China

Approved for public release; distribution is unlimited.

June 2007

DTRA 01-00-C-0048

Jiakang Xie

Prepared by:
Lamont-Doherty Earth Observatory of Columbia University
61 Route 9W
Palisades, NY 10964

DESTRUCTION NOTICE

FOR CLASSIFIED documents, follow the procedures in DoD 5550.22-M, National Industrial Security Program Operating Manual, Chapter 5, Section 7 (NISPOM) or DoD 5200.1-R, Information Security Program Regulation, Chapter 1X.

FOR UNCLASSIFIED limited documents, destroyed by any method that will prevent disclosure of contents or reconstruction of the document.

Retention of this document by DoD contractors is authorized in accordance with DoD 5220.22-M, Industrial Security Manual.

PLEASE NOTIFY THE DEFENSE THREAT REDUCTION AGENCY, ATTN: CST, 8725 JOHN J. KINGMAN ROAD, STOP-6201, FT BELVOIR, VA 22060-6201, IF YOUR ADDRESS IS INCORRECT, IF YOU WISH IT DELETED FROM THE DISTRIBUTION LIST, OR IF THE ADDRESSEE IS NO LONGER EMPLOYED BY YOUR ORGANIZATION.

DISTRIBUTION LIST UPDATE

This mailer is provided to enable DTRA to maintain current distribution lists for reports. (We would appreciate you providing the requested information.)

- ☐ Add the individual listed to your distribution list.
- ☐ Delete the cited organization/individual.
- ☐ Change of address.

Note:
Please return the mailing label from the document so that any additions, changes, corrections or deletions can be made easily. For distribution cancellation or more information call DTRA/CST (703) 767-4725.

NAME: _____

ORGANIZATION: _____

OLD ADDRESS	NEW ADDRESS
_____	_____
_____	_____
_____	_____

TELEPHONE NUMBER: ( ) _____

DTRA PUBLICATION NUMBER/TITLE	CHANGES/DELETIONS/ADDITONS, etc. *(Attach Sheet if more Space is Required)*
_____	_____
_____	_____
_____	_____

DTRA or other GOVERNMENT CONTRACT NUMBER: _____

CERTIFICATION of NEED-TO-KNOW BY GOVERNMENT SPONSOR (if other than DTRA):

SPONSORING ORGANIZATION: _____

CONTRACTING OFFICER or REPRESENTATIVE: _____

SIGNATURE: _____

REPORT DOCUMENTATION PAGE

Form Approved
OMB No. 0704-0188

1. REPORT DATE *(DD-MM-YYYY)*	**2. REPORT TYPE**	**3. DATES COVERED** *(From - To)* 06/29/00 - 06/29/03
4. TITLE AND SUBTITLE A Study of Long-Range Seismic Profile Data in Western China		**5a. CONTRACT NUMBER** DTRA 01-00-C-0048
		5b. GRANT NUMBER DTRA 01-00-C-0048
		5c. PROGRAM ELEMENT NUMBER B62D
6. AUTHOR(S) Jiakang Xie		**5d. PROJECT NUMBER** CB
		5e. TASK NUMBER CB
		5f. WORK UNIT NUMBER DH12468
7. PERFORMING ORGANIZATION NAME(S) AND ADDRESS(ES) Lamont-Doherty Earth Observatory of Columbia University in the City of New York 61 Route 9W Palisades, New York 10964		**8. PERFORMING ORGANIZATION REPORT NUMBER** I
9. SPONSORING / MONITORING AGENCY NAME(S) AND ADDRESS(ES) Defense Threat Reduction Agency 8725 John J. Kingman Road, MS 6201 Fort Belvior, VA 22060-6201		**10. SPONSOR/MONITOR'S ACRONYM(S)**
		11. SPONSOR/MONITOR'S REPORT NUMBER(S) DTRA - TR-05-30
12. DISTRIBUTION / AVAILABILITY	Approved for public release; distribution is unlimited.	

13. SUPPLEMENTARY NOTES This work was sponsored by the Defense Threat Reduction Agency under RDT&E RMC code B B62D D H000 CB CB 12468 25904D.

14. ABSTRACT

Pn spectra are collected from three seismic experiments in the Tibetan Plateau (TP), over four path groups.The first and second path groups run southward from the eastern Tarim Basin
to stations in north and south central Tibet. The third and fourth path groups form two NNE-oriented profiles in the eastern TP. Events recorded by the first 2 path groups are also recorded by the Khyrghistan network (KNET) to the west. A comparison of Pn spectra averaged over both path groups and KNET reveal that mantle lid under the TB attenuates P waves more severely than central Asia, particularly at high frequencies (> 1 Hz). Apparent Q0 and z (Pn Q at 1 Hz and its frequency dependence, respectively) are estimated with a simplified geometrical spreading. Over path group 1 that heavily samples northern TB, Q0 and z are estimated to be 183+-33 and 0.3+-0.1, respectively. Over path groups 2 and 3 that sample either a mixture of northern and southern Tibet or eastern Tibet, the estimated Q0 and z are between 250 and 270 and 0.0 and 0.1, respectively. Over the fourth path group that sample the easternmost TB the respective estimates are 374+-51 and 0.3+-0.1. A comparison of Pn attenuations in continental regions suggest that they are similar in the easternmost TB, central Asia, Scandinavia and Canadian shield. Northern Tibet has the highest attenuation at all frequencies. Pn attenuation under southern Tibet is similar to the shield regions at low frequencies (<= 1Hz), and similar to northern Tibet at higher frequencies (up to 4 Hz). It appears that a southward increase in the lid temperature causes increases of both Pn velocity and low-frequency Pn Q, but causes no change of high-frequency Pn Q. This phenomenon may be best explained by a propagation mechanism in which Pn traverses the lid as a single, deep refraction at low frequencies, and as multiply bounced and scattered ("whispering-gallery") rays at high frequencies

15. SUBJECT TERMS Pn, Tibetan Plateau, Attenuation, Q, Seismic Spectra, Upper Mantle			
16. SECURITY CLASSIFICATION OF: Unclassified	**17. LIMITATION OF ABSTRACT**	**18. NUMBER OF PAGES**	**19a. NAME OF RESPONSIBLE PERSON** Jiakang Xie
a. REPORT **b. ABSTRACT** **c. THIS PAGE**	SAR	41	**19b. TELEPHONE NUMBER** *(include area code)* 845-365-8553

CONVERSION TABLE

Conversion Factors for U.S. Customary to metric (SI) units of measurement.

MULTIPLY →	BY →	TO GET
TO GET ←	BY ←	DIVIDE

angstrom	1.000 000 x E -10	meters (m)
atmosphere (normal)	1.013 25 x E +2	kilo pascal (kPa)
bar	1.000 000 x E +2	kilo pascal (kPa)
barn	1.000 000 x E -28	meter^2 (m^2)
British thermal unit (thermochemical)	1.054 350 x E +3	joule (J)
calorie (thermochemical)	4.184 000	joule (J)
cal (thermochemical/cm^2)	4.184 000 x E -2	mega joule/m^2 (MJ/m^2)
curie	3.700 000 x E +1	*giga bacquerel (GBq)
degree (angle)	1.745 329 x E -2	radian (rad)
degree Fahrenheit	$t_k = (t°f + 459.67)/1.8$	degree kelvin (K)
electron volt	1.602 19 x E -19	joule (J)
erg	1.000 000 x E -7	joule (J)
erg/second	1.000 000 x E -7	watt (W)
foot	3.048 000 x E -1	meter (m)
foot-pound-force	1.355 818	joule (J)
gallon (U.S. liquid)	3.785 412 x E -3	meter^3 (m^3)
inch	2.540 000 x E -2	meter (m)
jerk	1.000 000 x E +9	joule (J)
joule/kilogram (J/kg) radiation dose absorbed	1.000 000	Gray (Gy)
kilotons	4.183	terajoules
kip (1000 lbf)	4.448 222 x E +3	newton (N)
kip/inch^2 (ksi)	6.894 757 x E +3	kilo pascal (kPa)
ktap	1.000 000 x E +2	newton-second/m^2 ($N-s/m^2$)
micron	1.000 000 x E -6	meter (m)
mil	2.540 000 x E -5	meter (m)
mile (international)	1.609 344 x E +3	meter (m)
ounce	2.834 952 x E -2	kilogram (kg)
pound-force (lbs avoirdupois)	4.448 222	newton (N)
pound-force inch	1.129 848 x E -1	newton-meter (N-m)
pound-force/inch	1.751 268 x E +2	newton/meter (N/m)
pound-force/foot^2	4.788 026 x E -2	kilo pascal (kPa)
pound-force/inch^2 (psi)	6.894 757	kilo pascal (kPa)
pound-mass (lbm avoirdupois)	4.535 924 x E -1	kilogram (kg)
pound-mass-foot^2 (moment of inertia)	4.214 011 x E -2	kilogram-meter^2 ($kg-m^2$)
pound-mass/foot^3	1.601 846 x E +1	kilogram-meter^3 (kg/m^3)
rad (radiation dose absorbed)	1.000 000 x E -2	**Gray (Gy)
roentgen	2.579 760 x E -4	coulomb/kilogram (C/kg)
shake	1.000 000 x E -8	second (s)
slug	1.459 390 x E +1	kilogram (kg)
torr (mm Hg, 0° C)	1.333 22 x E -1	kilo pascal (kPa)

*The bacquerel (Bq) is the SI unit of radioactivity; 1 Bq = 1 event/s.
**The Gray (GY) is the SI unit of absorbed radiation.

Table of Contents

Figures

Tables

Section 1

Executive Summary

Pn spectra are collected from three PASSCAL seismic experiments in the Tibetan Plateau (TP), over four path groups. The first and second path groups run southward from events in the eastern Tarim Basin (ETB), to stations in north and south central Tibet. The third and fourth path groups form two NNE-oriented profiles in the eastern TP. Events recorded by the first 2 path groups are also recorded by the Khyrghistan network (KNET) to the west. A comparison of Pn spectra averaged over both path groups and KNET reveal that mantle lid under the TB attenuates P waves more severely than central Asia, particularly at high frequencies (> 1 Hz). Apparent Q_0 and η (Pn Q at 1 Hz and its frequency dependence, respectively) are estimated with a simplified geometrical spreading of $\Delta^{-1.3}$. Over path group 1 that heavily samples northern TB, Q_0 and η are estimated to be 183±33 and 0.3±0.1, respectively. Over path groups 2 and 3 that sample either a mixture of northern and southern Tibet or eastern Tibet, the estimated Q_0 and η are between ~250 and 270 and 0.0 and 0.1, respectively. Over the fourth path group that sample the easternmost TB the respective estimates are 374±51 and 0.3±0.1, similar to the estimates of 364 and 0.5 for central Asian paths from ETB to KNET. A comparison of Pn attenuations in continental regions suggest that they are similar in the easternmost TB, central Asia, Scandinavia and Canadian shield. Northern Tibet has the highest attenuation at all frequencies. Pn attenuation under southern Tibet is similar to the shield regions at low frequencies (≤ 1Hz), and similar to northern Tibet at higher frequencies (up to 4 Hz). It appears that a southward increase in the lid temperature causes increases of both Pn velocity and low-frequency Pn Q, but causes no change of high-frequency Pn Q. This phenomenon may be best explained by a propagation mechanism in which Pn traverses the lid as a single, deep refraction at low frequencies, and as multiply bounced and scattered ("whispering-gallery") rays at high frequencies.

Section 2

Pn Attenuation beneath the Tibetan Plateau

2.1 Introduction

Pn is the first arriving high-frequency seismic phase at regional distances between about 2-15°. At close distances Pn can be modeled as a pure mantle head wave, which evolves into a mantle turning wave with increasing distance (*e.g.,* Sereno and Given, 1990). This peculiar wave evolution causes the features of Pn, such as its ray geometry, travel time and amplitude vary with distance in manners that are highly dependent on the velocity gradient in the mantle lid. Simplifications to these variations are typically introduced when Pn is used to study the velocity and attenuation structure of the mantle lid. Pn arrival times have been extensively used to study the lateral variations of compressional wave velocity (v_p) in the lid (e.g., Hearn et al., 1986). Most studies have ignored effects of the mantle velocity gradient and treated Pn as a pure head wave at all distances. A few studies, such as Zhao and Xie (1993) and Hearn et al. (2004) accommodated the first-order effect of velocity gradient and obtained v_p models that vary both laterally and vertically in the mantle lid.

Few studies have been conducted to use Pn amplitude to estimate the other important seismic parameter, Q. A fundamental difficulty in estimating Pn Q is caused by the lack of knowledge of the geometrical spreading term (G.S.T.), which describes the Pn amplitude fall-off with distance owing to the wavefront expansion in the mantle lid. The Pn G.S.T. is very sensative to details of of the lid velocity structure. Sereno and Given (1990) and Xie (1996) estimated the G.S.T. of Pn for Scandinavia and central Asia using synthetic seismograms calculated for various 1D velocity models. They found even for these simplified models the G.S.T. varied with distance and frequency in rather complex manners. In the real, 3D Earth structure even more complications are expected. For example, scattering and multiple bouncing (whispering-gallery) processes may affect the Pn wavetrain (e.g., Menke and Richards, 1980, 1983). To tackle the uncertainty in G.S.T., different parameterizations have been used in studies of Pn amplitude attenuation. Sereno et al. (1988) and Xie and Patton (1999) assumed a simplified, frequency independent G.S.T. of $\Delta^{-1.3}$ and estimated models of Pn Q ($Q(f)$) in Scandinavia and central Asia. They assumed a power-law frequency dependence of Pn Q, $Q(f) = Q_0 f^{\eta}$, where Q_0 and η are Pn Q at 1 Hz and its frequency dependence, respectively. They obtained similar Q_0 values of 325 and 364, and η values of ~0.5 for the two regions. Zhu et al. (1991)

simultaneously estimated a frequency-dependent G.S.T. and $Q(f)$ for Canadian shield. Other authors (e.g., Tinker and Wallace, 1997) simply parameterized Pn attenuation by a single G.S.T. without Q.

The mantle lid under the Tibetan plateau is known to have highly laterally variable P wave velocities (v_p). Zhao and Xie (1993), McNamara et al. (1997) and Hearn et al. (2002) used Pn arrival time data to invert for the laterally varying v_p models. Their v_p models contain grossly similar features such as a zone of low v_p under northern Tibet, and high v_p under much of southern Tibet. Ni and Barazangi (1983) and McNamara et al. (1995) also found that the Sn wave, which is the shear wave that traverses the mantle lid similarly to Pn, seemed to suffer abnormally high attenuation under northern Tibet. These findings are used to infer that the mantle lid is hot and partially molten under a broad region in northern Tibet, and cold under southern Tibet. Results of Pn and Sn studies, when jointly used with those of studies of other geophysical quantities, lead to the geodynamic model in which the Indian lithosphere underthrusts in southern Tibet (Nelson et al., 1996), and subducts into the mantle further south, along the latitude of ~32°N (Tilmann et al., 2003). Measurements of Sn attenuation under Tibet has been conducted qualitatively, by examining whether the amplitude ratio of Sn to P coda is above a threshold value such as 1 (Ni and Barazangi, 1983; McNamara et al., 1995). This is because when the Sn is weak or P coda is strong, it is not practical to estimate the true Sn amplitude. By contrast, spectral amplitudes of Pn wavetrain can be calculated in the distance range where Pn is the first arrival. In this paper we present analyses of Pn spectra recorded during three PASSCAL experiments in Tibet. We first compare Pn spectra from three events that occurred in 1994 or 1999 in the eastern Tarim Basin, which are simultaneously recorded by the INDEPTH (International Deep Profiling of Tibet and the Himalaya) II or III stations to the south, and Khyrghistan network to the west. The comparison provides direct evidence that the mantle lid under the Tibetan Plateau is more attenuative than that under eastern Tienshan at high frequencies ($\geq$ 1 Hz). We then quantify the Pn attenuation along paths to INDEPTH networks by estimating apparent Pn Q under a simplified G.S.T. and omega-square source models. This is followed by two-station measurements of apparent Pn Q along two PASSCAL profiles in eastern Tibet, deployed during the 1991-1992 Tibetan Plateau experiment. We report a spatial trend for the apparent Pn Q_0 to be low in north central Tibet, and to increase both southward and eastward. This trend correlates with the spatial variation of apparent Pn velocity measured in previous and this studies. However, this spatial t rend of Pn Q variation tends to diminish at high frequencies (up to 4 Hz). We that suggest under the Plateau, the propagation and attenuation mechanisms of Pn and its coda may be frequency dependent. At higher frequencies

($\geq$ 1 Hz) Pn wavetrains may be more affected by multiple bouncings and scattering near the crustal/mantle boundary. Finally we compare the apparent Pn attenuations published for various continental regions in the world, in a manner that is independent of the G.S.T. used, to see how the attenuations are affected by various tectonic environments.

2.2 Data Processing

Figure 1 shows all seismic stations in Tibet deployed during the three PASSCAL experiments. The 1991-1992 Sino-US Tibetan Plateau experiment consisted of 11 broad-band stations that were deployed between July, 1991 and July, 1992 (Owens et al., 1993), in the eastern part of the Tibetan plateau. The INDEPTH II experiment was conducted in southern Tibet between May and October, 1994 (Nelson et al., 1996), with 9 broad-band and 6 short-period stations deployed along an NNE-oriented profile. The INDEPTH III experiment was conducted in central Tibet between July, 1998 and June, 1999. Forty-seven broad or intermediate band and 15 short-period stations were deployed along a profile across the Banggong-Nujiang Suture (BNS) in a NNW direction (Figure 1; also c.f. Rapine et al., 2003). Stations in all three experiments are three-component, with sampling rates of 20 s^{-1} or higher. Figure 1 also shows the locations of regional events used in this study. Figure 2 shows an example of the record sections containing Pn.

To obtain stable estimates of Pn amplitude spectra, a finite-length Pn wavetrain that includes Pn coda must be used (Sereno et al., 1988; Zhu et al., 1991; Xie and Patton, 1999). In this study we follow the procedure by these authors to compute average spectra of Pn and Pn coda, using spectra from a series of overlapping windows applied to the vertical-component seismograms. These windows have a constant length of 4.5 s, a 20% taper and 50% overlap. Only spectra with signal noise ratios larger than 2 are used. The maximum number of the windows for a given seismogram is determined by the following criteria: (a) the total length of Pn wavetrain sampled does not exceed 12.5 s (i.e., the maximum window number is 5), (b) at closer distances (Δ < 1000 km) the last window does not include signals with group velocities slower than 6.6 km/s, so the crustal Pg wave is not sampled (Xie and Patton, 1999); and (c) at large recording distances (Δ~1500 km) the last window does not include the possible reflections from the 440 km and 660 km discontinuities, previously observed in Tibet (8301 Program Group, 1988). Figure 3 shows an example of the windows used, and the resulting individual and average Fourier spectra of the Pn wavetrain. The effect of ambient noise is reduced by subtracting the signal power by the noise power. Instrument responses are then removed. We shall refer to the average spectra thus calculated for the Pn wavetrain as "Pn spectra" in the rest of the report.

2.3 Pn Spectra from Events in the Eastern Tarim Basin

2.3.1. Spectra from the 1994 Explosions

During the INDEPTH II experiment, two underground nuclear explosions occurred in the eastern Tarim Basin, in the Lop Nor Test Site (Figure 1). Pn wavetrains are recorded by all 12 operational INDEPTH stations for the October 7 (Mb~6) explosion (Figure 2), and by 7 stations for the June 10 (Mb=5.7) explosion. Pn spectra from both explosions were also recorded by the Khyrghistan network (KNET) to the west (Figure 1), and studied by Xie and Patton (1999). The paths to the KNET stations traverse to the eastern Tienshan. In comparison, the paths to the INDEPTH II network run southward and sample the TB. Both groups of paths have similar, far-regional distances between about 1050 and 1550 km (Figure 1). Any anisotropic radiation patterns are expected to be minimal for the Pn wavetrain. Therefore we may directly compare the Pn spectra to see the gross attenuation effect of the mantle lid under Tienshan and the Tibetan Plateau. The top two rows of Figure 3 show the Pn ground displacement spectra from both explosions, scaled by $\Delta^{1.3}$ to reduce the effects of G.S.T.

A prominent feature of the Pn spectral amplitudes from both explosions is their variability within the networks, particularly within the KNET. Both networks have apertures of less than about 350 km compared to the average path lengths of > 1050 km. Yet the sample standard deviation is typically at the level of ~60% of the averaged spectra for the KNET stations, and range between ~60% (at frequencies < 1 Hz) and ~30% (at frequencies > 1 Hz) for the INDEPTH stations. The time-domain amplitudes of the first Pn pulses are even more variable. For example, for the October 7 explosion the peak Pn amplitudes vary by a factor of 19 across the KNET (Figure 3 of Xie and Patton, 1999) and by a factor of 4 across the KNET (Figure 2). For both networks the amplitude variations are not monotonic with distance, so path attenuation from finite Q is not the primary cause of the variations. Xie (1996) and Xie and Patton (1999) concluded that the most likely cause for the drastic Pn amplitude variations across the KNET is a laterally varying Moho topography that likely occurred along the Tienshan range. Xie (1996) conducted ray tracings in 2D velocity models for Central Asia in and around the Tienshan region to demonstrate the potential effect of a Moho topography. Significant amplitude variations of Pn over short distance ranges seem to be common in other mountainous regions. For example, Tinker and Wallace (1997) reported such a variation in the western U.S. and modeled it as being the caused by structural complications that likely involved Moho topographies. The use of a finite duration wave train to calculate Pn spectra has not sufficiently suppressed its

variability. Therefore to study the gross effect of whole-path attenuations, we take the network average of Pn spectra, as shown in the right columns of Figure 3. We also calculate the sample standard deviation of Pn spectra within each network as a statistical measure of their variability.

The network-averaged Pn spectra from the well recorded, October 7 explosion (top right panel of Figure 3) start at similar levels at the lowest frequency (~0.4 Hz). With increasing frequency the average spectrum from the INDEPTH II network rapidly falls below that from the KNET. At ~1 Hz the separation between the two spectra reaches a factor of 4. At higher frequencies the separation increases monotonically with frequency and overwhelms the variabilities within the networks as measured by the standard deviations. At 4 Hz (the highest frequency available for INDEPTH spectra), the separation reaches to a factor of ~35. Network averaged spectra from the June 10 explosion (rwo 2 right of Figure 4) have a similar, frequency-dependent separation, although the smaller event size causes both fewer recordings and narrower recording bands. Since the recording distances to KNET and INDEPTH networks are similar, the frequency dependent separations between the network-averaged Pn spectra from both explosions mean that Pn attenuations under the Tibetan plateau and Tienshan are similar at low frequencies (~0.4 Hz), but become increasingly different with increasing frequency.

2.3 Pn Spectra from Events in the EasternTarim Basin

2.3.2 Spectra from the 1999 earthquake

Event "99.030" in Figure 1 is an m_b=5.9 earthquake on January 30, 1999, which nearly colocated with the 1994 explosions. The event is simultaneously recorded by 10 KNET and 38 INDEPTH III stations. Of the the latter, 35 are deployed along a main profile that crosses the BNS, and 3 are deployed on the BNS but outside the main profile (Figures 1 and 5). Pn velocity analyses reveal that the BNS is an approximate boundary separating regions of abnormally slow and fast mantle lid velocities (Zhao and Xie, 1993; McNamara et al., 1997; Hearn et al., 2002; also see APPENDIX B of this paper). So in this study we have divided the INDEPTH III stations into two groups. Group 1 (denoted as III-1) contains stations south of the BNS and group 2 (denoted as III-2) contains stations north of, and on, the BNS (Figure 5). Rows 3 and 4 of Figure 4 show the Pn spectra from KNET and the two groups of INDEPTH III stations. As in the case of Pn spectra from the explosions (top two rows in Figure 4), the spectra from earthquakes (bottom two rows) also exhibit substantial variations within each network, particularly the KNET. The averages of Pn spectra from KNET and INDEPTH III stations also exhibit a frequency-dependent separation, indicating more severe attenuation of the Tibetan mantle lid at higher frequencies. There are also notable differences between explosion and earthquake

spectra. First the explosion spectra contains spectral overshoots near the source corner frequencies (e.g., above 1 Hz for the October 7 explosion). The earthquake spectra (bottom rows) exhibit no overshoot and decay more gently (see Xie and Patton, 1999 for a detailed discussion). Second, the earthquake spectra may be affected by a potential non-isotropic source radiation pattern. We believe the radiation pattern is small in the spectra but will delay the discussion to a later section.

2.4 Stochastic Modeling of Pn Spectra

To quantitatively estimate Pn Q and source spectra, we use the stochastic modeling of Pn spectra used by Sereno et al. (1988) and adapted by Xie and Patton (1999). For convenience we briefly summarize the modeling here. We assume that Pn spectra, $A(f)$, can be modeled by $A(f) = S(f)R(\theta)G(\Delta)\exp\left(-\frac{\pi f \Delta}{VQ(f)}\right)X(f)$, where θ, Δ, V are the azimuth, distance and Pn group velocity, respectively. $Q(f)$ is Pn Q (equation (1)). $R(\theta)$ is the source radiation pattern. $X(f)$ is an error term that represents systematic errors such as a non-unity site response, and random errors caused by amplitude fluctuation (note here we use $X(f)$ to represent the combined effect of site response and random term in equation (1) of Xie and Patton, 1999 for simplicity). $S(f)$ is the Pn source spectrum, which is given by the Brune's model and Modified Mueller-Murphy (MMM) model for earthquakes and explosions, respectively (equation (2) of Xie and Patton, 1999). Both models have f^{-2} asymptotic decays at high-frequencies, and are grossly characterized by a seismic moment (M_0) and corner frequency (f_c). The MMM model for explosions also has a spectral overshoot controlled by a parameter β, which is set as 1.0 by Xie and Patton (1999). In equation (2), $G(\Delta)$ is the geometrical spreading term (G.S.T.) and takes the form, $G(\Delta) = \Delta_0^{-1}(\Delta_0/\Delta)^m$ where Δ_0 is a reference distance, and m is the decay rate of $A(f)$ at large distances ($\Delta > \Delta_0$). As mentioned in the Introduction, a well known problem in modeling Pn is that the values of Δ_0 and m are uncertain because of the unknown details of the lid velocity structure. Sereno *et al.*, (1988) used Δ_0 and m of 1 km and 1.3, respectively, for Scandinavia. Xie (1996) found that these values were within the ranges obtained using synthetic Pn waveforms in various 1D velocity models for central Asia. Xie and Patton (1999) used these Δ_0 and m values to study Pn spectra from several nearly colocated explosions in the eastern Tarim Basin (ETB), recorded by the KNET in the west, and the Kazakhstan network (KZNET) in the north. Applying a non-linear, Bayesian inverse method to these spectra, Xie and Patton (1999) simultaneously estimated source M_0, f_c and path-variable Q_0 and η values to KNET and KZNET. These will be used as a priori knowledge in this study (next section).

2.5 Estimates of Pn Q to Indepth Stations

Xie and Patton estimated the M_0 and f_c values of the October 7 explosion to be 3.2×10^{15} Nm and 2.6 Hz, respectively. We use these values as a priori knowledge to estimate path-variable Q_0 and η values to the INDEPTH II stations (Equation (2), also see equation (13) of Xie and Patton, 1999; note $R(\theta)$ should be ignorable for explosions). These Q_0 and η values are then averaged over all INDEPTH II stations. Figure 6 (row 1) shows the fit of the source spectral and path Q models to the observed Pn spectra from the INDEPTH II network and KNET. At 1 Hz, the average Pn Q_0 to the INDEPTH II stations is estimated to be 253±53, which is about 30% lower than the value of 364 to KNET stations estimated by Xie and Patton (1999). The average η to INDEPTH II stations is 0.0±0.1, which is much lower than the average η of 0.5 estimated to the KNET stations. The June 10 explosion are relatively poorly recorded, in narrower frequency bands and by only a fraction of the stations (Figure 4). We are not confident at estimating Q using that event.

To estimate Pn Q from earthquake 99.030 to the INDEPTH III stations, as well as the source M_0 and f_c values, we use the average (Q_0, η) values of (364, 0.5) to KNET, estimated by Xie and Patton (1999), as a priori knowledge. We use this knowledge to correct for path effects in the KNET spectra, and obtain estimates of source M_0 and f_c values of 2.49×10^{16} Nm and 0.8 Hz, respectively. We then make an assumption that the source radiation pattern does not vary significantly from the INDEPTH III direction to the KNET direction, so that the Q_0 and η values to the former stations can be estimated using the above M_0 and η values obtained using KNET spectra ignoring $R(\theta)$ (equation (2)). We give an extensive discussion on the validity of this assumption to APPENDIX A. Under this assumption, the average Q_0 and η values to the southern station group, III-2, are estimated to be 255±48 and 0.1±0.1. These values are similar to those to the INDEPTH II stations estimated above. By contrast, the average Q_0 and η values to station group III-1, located to the north of BNS, are estimated to be 183±33 and 0.3±0.1, respectively.

The Q_0 and η estimates presented in this section are those along long paths from ETB and contain small crustal segments in both the source and receiver end, and small mantle segments in the Tarim Basin. Xie et al. (2004) estimate Q of crustal Lg waves within the INDEPTH II and III networks by using the two-station method, which minimizes effects of both attenuation outside the networks and the source radiation. We attempted to use the two-station method to estimate Pn Q along the INDEPTH profiles but obtained very unstable (negative) Q values. This is

likely caused by the large variability of Pn spectral amplitudes within the INDEPTH II and III networks (Figure 4) which means errors ($X(f)$ in equation (2)) are large. Xie et al. (2004) pointed out that at a given frequency, the effect of error ($X(f)$) in Q estimates could be suppressed by using large measuring distances. Unfortunately the INDEPTH profiles are short (< 350 or 400 km; see Figure 1), resulting in small inter-station distances that are not adequate to suppress the large $X(f)$.

2.6 Pn Q Along Passcal Profiles in Eastern Tibet

Stations deployed during the 1991-1992 Sino-US Tibetan Plateau experiment (Owens et al., 1993, BSSA) recorded Pn spectra from four regional earthquakes (Figures 1 and 5) that are approximately in line with profiles SANG-TUNL and SANG-MAQI in eastern Tibet. For these spectra no source M_0 and f_c values are available so we must rely on the two-station method to estimate Pn Q. Inter-station distances along these two profiles are generally large so the effect of error term ($X(f)$) in Q measurements should be reduced (last section). We use Pn spectra along these profiles to estimate spectral ratios from many pairs of two-stations. We find that ratios from event 91.257 estimated along profile TUNL-SANG (Figure 5) are unstable, yielding negative inter-station Pn Q values. Zhu and Helmberger (1998) used teleseismic data to infer that the Moho north of station TUNL has a drastic depth-offset of at least 15-20 km. Pn spectral amplitudes along profile TUNL-SANG, from event 91.257, are likely affected by diffractions from this Moho offset, resulting in the observed instability in their ratios. We do not use these spectra in the subsequent Q estimates.

The rest of Pn spectral ratios are averaged along profiles SANG-TUNL, SANG-MAQI and WNDO-TUNL to estimate Q_0 and η using equation (4) of Xie et al. (2004), replacing V_{Lg} by a Pn group velocity of 7.6 km/s. Profile WNDO-TUNL is actually the northern half of profile SANG-TUNL; it is used to see if Pn Q changes from south to north along profile SANG-TUNL that crosses the BNS. Figure 7 shows the stacked spectral ratios (SSRs) along the three profiles and the best fitting Q_0 and η values. At most frequencies ($>$ 0.7 Hz) the SSRs closely follow the straight lines representing the best fitting models of Q_0 and η. The SSRs at frequencies lower than 0.7 Hz are abnormally small along all profiles. These may be caused a trend of increasing effects of modeling errors ($X(f)$) in Q estimates toward lower frequencies, as predicted by Xie et al. (2004). The Q_0 and η values estimated along profile SANG-TUNL are 278±23 and 0.1±0.1, respectively (Figure 7), similar to those estimated for paths from the ETB to the INDEPTH stations in southern Tibet (last section). There is no significant north-south change of Q_0 and η values along profile SANG-TUNL since the values estimated along its northern half (profile WNDO-TUNL) are 273±32 and 0.0±0.1 (Figure 7), virtually the same as those estimated along the entire profile. The Q_0 and η estimated along profile SANG-TUNL, which is located in the easternmost TB, are about 374±57 and 0.3±0.1, similar to the the values of 364 and 0.5 estimated for paths from the ETB to KNET (Xie and Patton, 1999, also see the last section).

2.7 A Comparison of Pn Attenuation in Continental Regions

Figure 5 summarizes all Q_0 and η values estimated in this study and Xie and Patton (1999) for regions in and around the Tibetan plateau and Tienshan. Paths from eastern Tarim Basin (ETB) to north central Tibet are associated with the lowest Q_0 (~183). Higher Q_0 values are found along paths from ETB to south central Tibet, and along the two profiles in eastern Tibet. This trend of Q_0 increase from northern Tibet to southern and eastern Tibet will be further discussed later, after we broaden the comparison of Pn attenuations to include those from other continental regions.

Because of the difficulties in obtaining stable Pn amplitude measurements and reliable Pn G.S.T., there have been few publications documenting Pn attenuation on continents to far-regional distance ranges. The few published models of Pn attenuation, or Q, are obtained using different G.S.T. (Sereno et al., 1988; Zhu et al., 1991; Tinker and Wallace, 1997; Xie and Patton, 1999). To compare them with those obtained in this study, we calculate models of Pn attenuation in the frequency domain at a reference distance of 1200 km (Figure 8). The calculation simultaneously accounts for the G.S.T. used, and the estimated Pn Q models. For the ease to see the differences among the models, the lowest frequency used for the calculations is 0.1 Hz which is slightly lower than those used in most studies. Pn attenuation models are similar for the relatively stable regions where mantle Pn velocity are higher then 8.0 km/s, including the Canadian shield, Scandinavia, central Asia and easternmost Tibet. This is so despite that the G.S.T. used for the Canadian Shield by Zhu et al. (1991) has a frequency-dependent form of m=$1.07+0.035f$, rather than the form of m=1.3 used for Scandinavia, central Asia and easternmost Tibet.

The lowest model (corresponding to the strongest Pn attenuation) in Figure 8 is that for paths from ETB to northern Tibet (model "N. TP"). At all frequencies the model is below those for the stable regions, but the differences are more drastic toward higher frequencies. At 4 Hz the differences are more than a factor of 100. It is not surprising that of all the models compared, model N. TP has the strongest attenuation. As mentioned in the INTRODUCTION and APPENDIX B, analyses of lateral variations in Pn velocity have led to the inference that the temperature in the mantle lid under north central Tibet is abnormally low, probably reaching the solidus. Intrinsic Q is expected to be strongly, and monotonically, dependent on temperature and therefore should be very low in the mantle lid under north central Tibet, which is most heavily sampled by Model N. TP. What is surprising is that the in Figure 8, model C. CP. has a

very peculiar frequency dependence: that model is similar to those for stable regions at frequencies lower than ~1 Hz, but rapidly decreases toward higher frequencies such that at ~4 Hz, it becomes as low as model N. TB. Model C. TB. is developed for paths from ETB to southern Tibet (Figure 5) and partially samples the expected high intrinsic Q in the cold mantle lid beneath southern Tibet. If Pn attenuation dominantly reflects the intrinsic Q at all frequencies, we would expect model C. TB. to be higher then N. TB. at all frequencies, rather than just at frequencies below 1 Hz as shown in Figure 8.

A plausible explanation for the low level of model C. TB. at higher frequencies is that at these frequencies, the Pn wavetrain propagates with a different mechanism than at low frequencies. Menke and Richards (1980; 1983) proposed that the high frequency Pn wavetrain observed at teleseismic distances (up to 20°) may travel as a group of "whispering-gallery" phases that are multiply bounced and scattered near the Moho. The "whispering-gallery" mechanism has recently been used extensively to explain the puzzling observation of a high-frequency (> 2 Hz) Pn wavetrain at teleseismic distances of up to 3,000 km along the Soviet Peaceful Nuclear explosions (e.g, Morozov and Smithson, 2000; Neilsen and Thybo, 2003). The low-frequency Pn wavetrains from the ETB to Tibetan stations may propagate along deep-turning, refracted rays similar to those calculated for a 1D structure in Figure 9. They are much affected by the deep-seated anomalies of velocity and intrinsic Q in the mantle lid. Specifically, deep-seated low velocity, low Q mantle material under north central Tibet, and high velocity, high Q material under southern Tibet, might have caused the observed Pn velocity and low-frequency Pn Q to vary from north to south. On the other hand, if high-frequency Pn wavetrains propagate along the "whispering-gallery" rays similar to those shown in Figure 9, they may not be much affected by the deep-seated anomalies. Rather, they may be more affected by the 3D velocity and Q structures near the Moho, particularly the scattering in this region (Menke and Richards, 1983; Kvaerna and Doornbos, 1991; Ryberg et al., 1995; Morozov and Smithson, 2000). If this frequency-dependent Pn propagation mechanism is at work under much of the TB, then Pn attenuation may be dominantly affected by intrinsic Q at lower frequencies, and by scattering Q at higher frequencies.

2.8 Conclusions And Discussion

Pn attenuation is studied using data from three PASSCAL experiments in the Tibetan Plateau (TP), including the 1991-1992 Sino-US TP, the INDEPTH (International Deep Profiling of Tibet and the Himalaya) II and III experiments. Three seismic events in the eastern Tarim Basin (ETB) are simultaneously recorded by the INDEPTH II and III networks to the south and the Khyrghistan network (KNET) to the west, at similar far-regional distances ($\geq$ 1050 km). A comparison of the recorded Pn spectra yields direct evidence that the mantle lid under the TB is more attenuative than that under central Asia at high frequencies (> 1 Hz). At 4 Hz, the difference in attenuations cause the INDEPTH spectra to be about a factor of 35 smaller than the KNET spectra.

Under a simplified Pn geometrical spreading, we measure Q_0 and η (Pn Q at 1 Hz and its frequency dependence, respectively) along various path groups. For paths from ETB to northern Tibet we estimate Q_0, η to be 183±33 and 0.3±0.1, respectively. For paths to southern Tibet, and along a profile (SANG-TUNL) in eastern Tibet deployed during the 1991-1992 experiment, Q_0 increase to above 250, while η decrease to about 0.0. Along a profile in the easternmost Tibet (SANG-MAQI), Q_0 and η are 374±51 and 0.3±0.1, similar to those along central Asian paths from ETB to KNET. Lateral variations of Pn Q_0 has a pattern that is similar to those of Pn velocity and is consistent with an inferred hot mantle lid under north central TB.

A comparison of Pn attenuations in various continental regions suggests that they are similar in central Asia, easternmost TB, Scandinavia and the Canadian shield. Pn attenuation under southern and eastern Tibet has a peculiar frequency dependence: it is as low as that in the shield regions at low frequencies ($\leq$ 1Hz), and as high as that under northern Tibet at higher frequencies (up to 4 Hz). This peculiarity can be explained by a previously proposed propagation mechanism in which Pn traverses the mantle lid as a single refraction at low frequencies, and as multiply bounced and scattered, "whispering-gallery" waves at high frequencies. If this mechanism is at work under much of Tibet, then Pn Q may contain more contributions from intrinsic Q at lower frequencies, and from scattering Q at higher frequencies.

In theory, intrinsic P wave Q, Q_p, in the mantle lid is strongly affected by the temperature there. Caution must be taken in any attempts to infer lid temperature using Pn Q for three reasons. First, the estimated Pn Q are associated with an uncertainty caused by the imprecise G.S.T. used. Second, the estimated Pn Q may sample cumulative Q of various segments along Pn

estimated for paths to station group II. This preserved similarity empirically demonstrates that a potential bias in the the estimated Q_0 and η values, caused by a non-isotropic $R(\theta)$ from event 99.030, is small. As a further precaution, we repeated the procedure of estimating Q_0 and η values using the southern half (8) stations of the 15-station group III-2. These 8 stations are even closer to the INDEPTH II stations as they tend to overlap (Figures 1 and 5). We obtained average Q_0 and η estimates of 258±42 and 0.0±0.1, respectively. These values are similar to those obtained using all 15 III-2 stations and show that our empirical inference on small $R(\theta)$ is robust.

Section 3

Tables and Figures

Table 1. Pn Velocity Estimates

Profile or Network	Propagation Direction	Estimated Velocity (km/s)	Estimated Dip (°)
KNET	West	8.33±0.16	N/A
INDEPTH II	South	8.42±0.10	N/A
INDEPTH III(1)	South	7.71±0.11	N/A
INDEPTH III(2)	South	8.27±0.12	N/A
SANG-TUNL	two-way	8.17±0.14	0.8±0.7 to SW
WNDO-TUNL	two-way	8.13±0.20	2.5±1.0 to SW
SANG-MAQI	two-way	8.39±0.10	0.6±0.4 to SW

Propagation direction is the one along which Pn arrival times are read. A "two way" direction indicates that two-way arrival times are read for the velocity estimate, in which case approximate dips are also estimated using equation (4.53) of Telford et al. (1976).

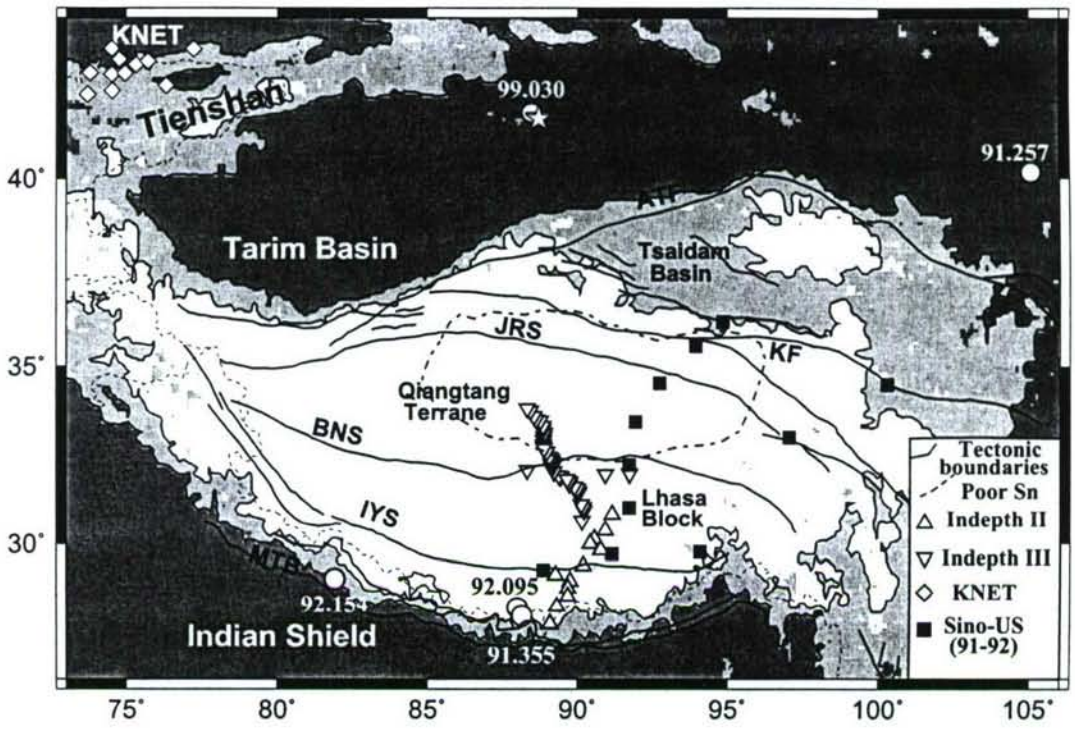

Figure 1. Map of study area. See inset annotation for symbols representing tectonic boundaries and seismic stations. The Sino-U.S. (91-92) and INDEPTH II and III stations were temporarily deployed during three PASSCAL experiments in Tibet. The Khyrghistan Network (KNET) is a permanent network. Regional earthquakes used in this study are showns as open circles. Earthquakes whose ID numbers start with 91 and 92 occurred in years 1991 and 1992 (see Table 2 of McNamara et al., 1995 for the event parameters). Earthquake 99.030 is an M_W=5.5 (m_b=5.9) event that occurred on January 30, 1999, at 3:51:5.4 UT. Stars are the June 10 and October 7, 1994 explosions (Table 1 of Xie and Patton, 1999). White, medium and dark grays represent elevations of greater than 4000 M, between 2000-4000M, and less than 2000 M, respectively. The abbreviations are: IYS - Indus Yalong Suture, BNS - Banggong-Nujiang Suture; JRS - Jinsha River Suture, KF - Kunlun Fault, ATF - Altyn Tagh Fault.

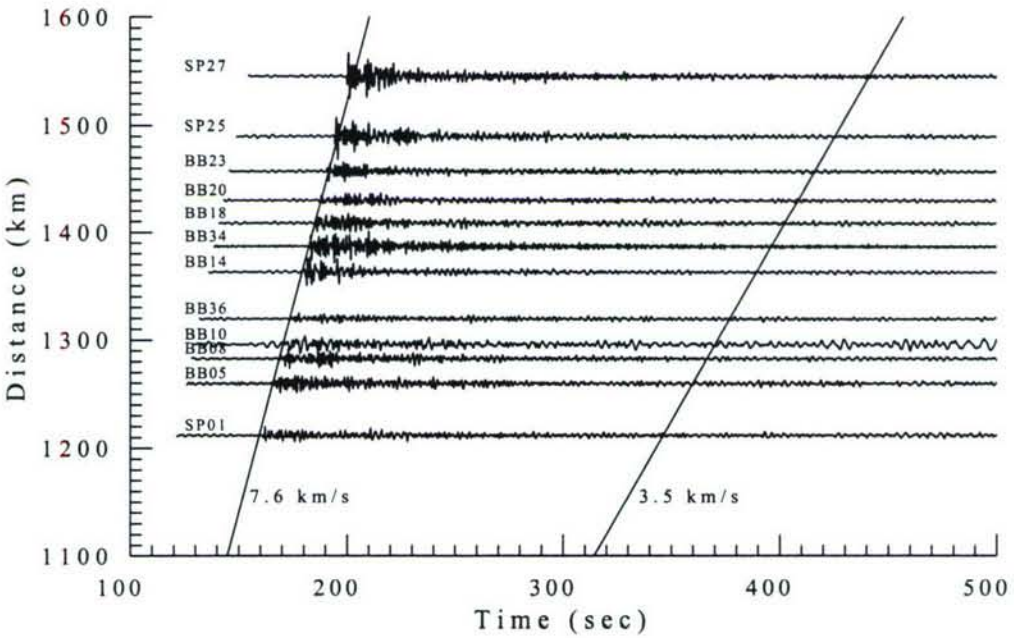

Figure 2. Vertical component record section from the INDEPTH II stations recording the October 7, 1994 explosion (m_b=5.9). Predicted arrival times corresponding to approximate Pn and Lg group velocities of 7.6 and 3.5 km/s are marked by gray lines. Lg is blocked. See Figure 3 of Xie and Patton (1999) for the record section from the KNET.

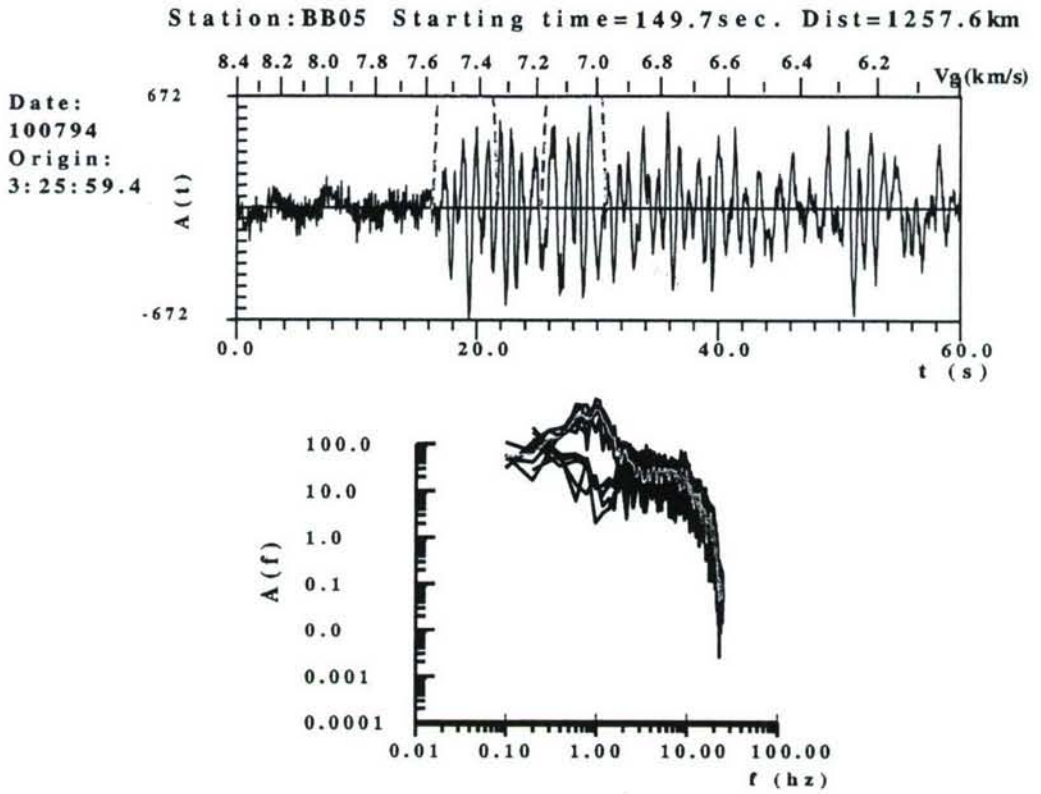

Figure 3. Time series containing the Pn wavetrain and the preceding noise (top), and Fourier spectra (bottom) from INDEPTH II station BB15 recording the October 7 explosion. For clarity, only two of the five signal windows (the first and third windows) are shown by the dashed curves on the top. Upper and lower black curves in the bottom are spectra from individual signal and noise windows. The spectrum in gray is the average of the Pn signal spectra.

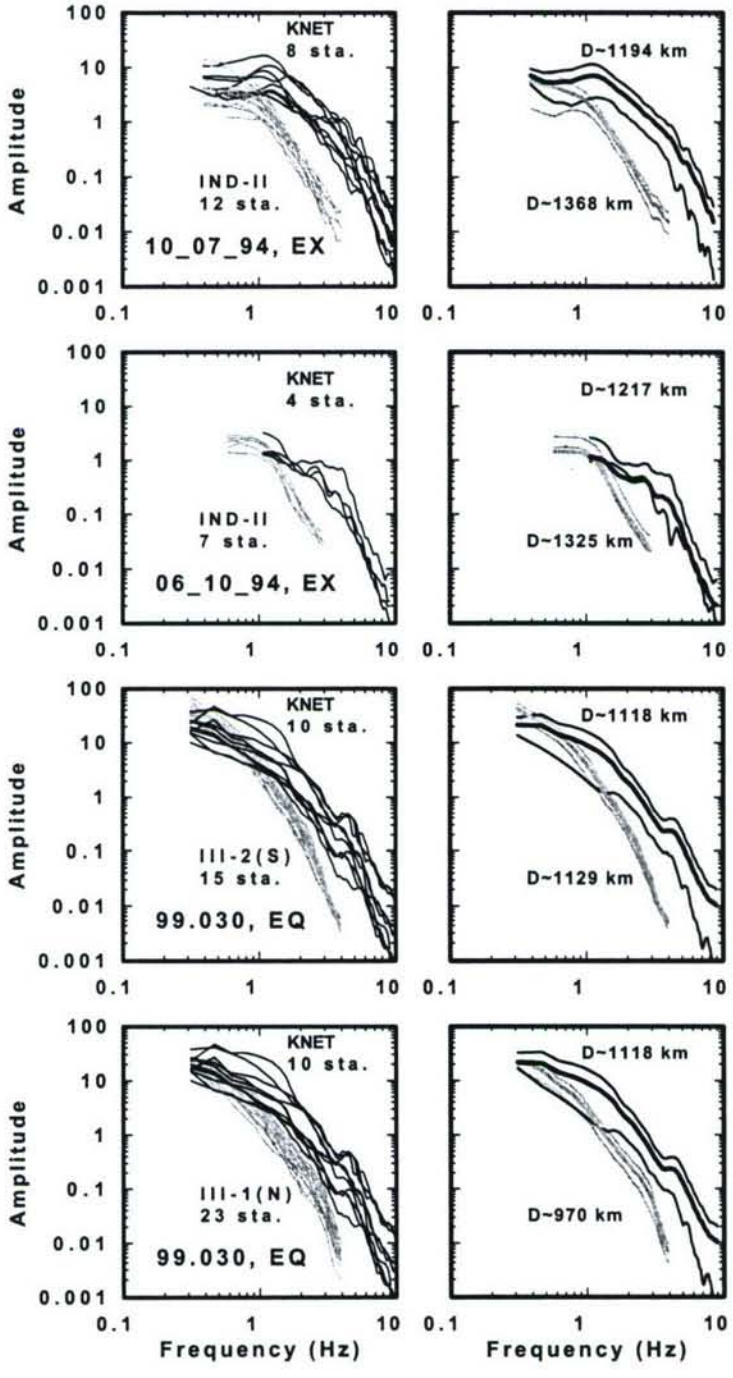

Figure 4. Pn spectra from explosions and earthquake in the eastern Tarim Basin (ETB). Spectra are scaled by $\Delta^{1.3}$ to reduce the effect of geometrical spreading. Each row is from one event as indicated at lower left, with "EX" and "EQ" indicating explosions and earthquake (see Figure 1). The INDEPTH III stations are divided into two groups (III-2 in row 3 and III-1 in row 4), located to the south and north of the BNS (Figures 1 and 5). Left columns show individual spectra from KNET and INDEPTH networks as black and gray curves, with the network name and number of recording stations written nearby. Right columns show the network averaged spectra and the associated sample standard deviations. The average distances are marked.

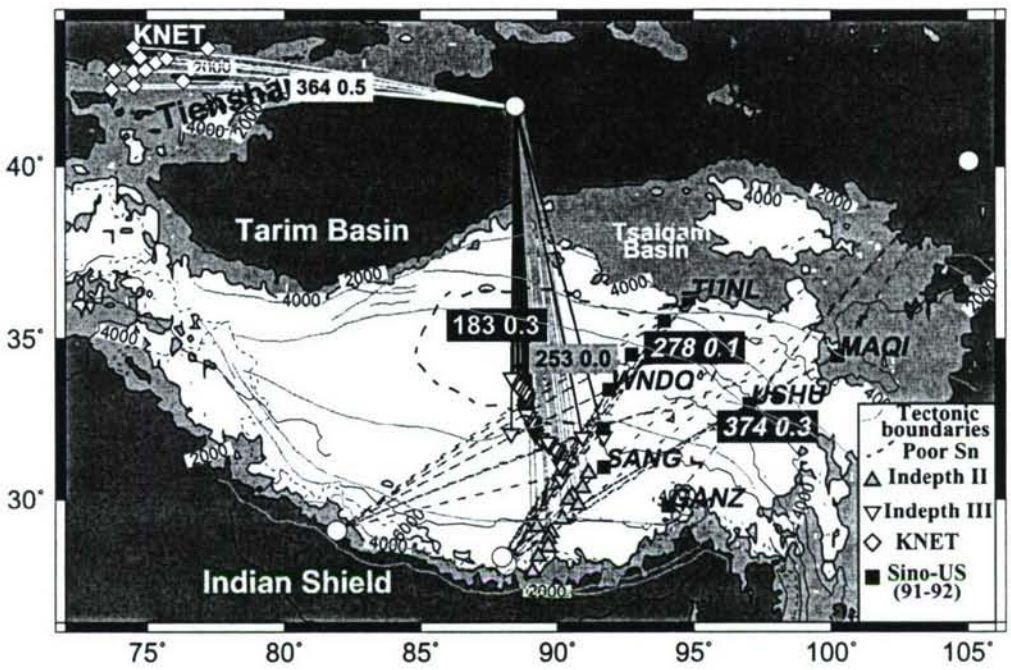

Figure 5. Map showing paths used in this study and the estimated Pn Q_0 and η values. The events and stations are the same as those plotted in Figure 1. Black paths are from earthquake 99.030 to station group III-2, sampling the northern Tibetan Plateau. Light gray paths are those from the 1994 explosions to INDEPTH II stations, or from earthquake 99.030 to station group III-1, sampling a mixture of northern and southern Tibetan Plateau. White paths are from explosions and earthquake 99.030 to KNET. Dashed lines plotted in darker gray are paths from the regional earthquakes to the 1991-1992 PASSCAL stations, used in the two-station Pn Q measurements. The end stations along profiles SANG-TUNL, WNDO-TUNL and SANG-MAQI are written (see McNamara et al., 1995 for other station names). The Pn Q_0 and η values are written near the paths over which they are estimated; oblique numbers are those obtained using the two-station method.

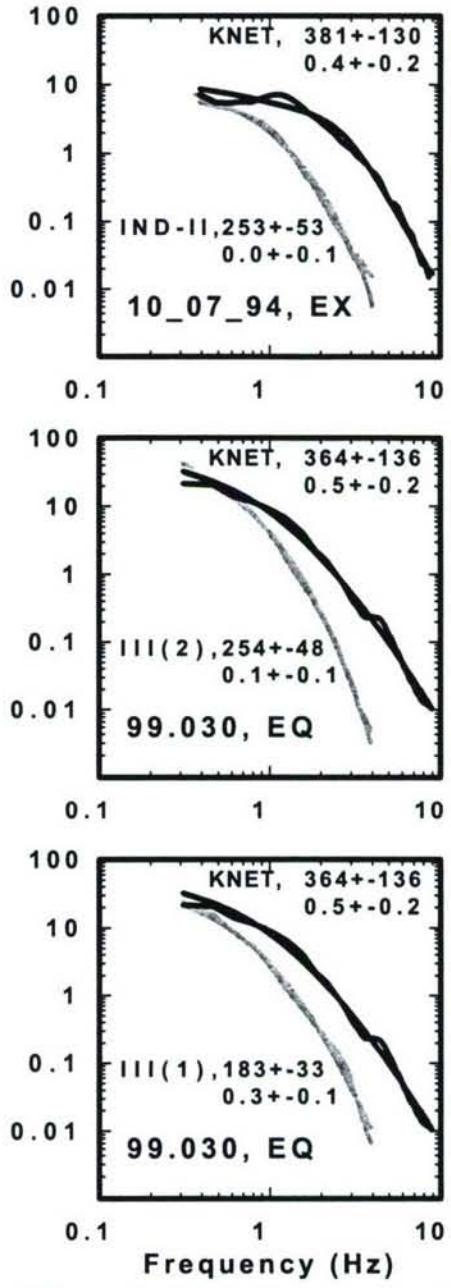

Figure 6. Network averaged Pn spectra (fluctuating curves), and the model spectra (smooth curves) corresponding to rows 1, 3 and 4 of Figure 4. Model spectra are constructed using the MMM or Brune source model, the estimated source M_0, f_c and path-averaged Q_0 and η values. Similarly to Figure 4, black and gray are used for spectra from KNET and INDEPTH networks. The network name and path-averaged Q_0 and η values are written near the curves. Note that only 8 KNET stations recorded the October 7 explosion, so the average Q_0 is 381, rather 364 obtained using all 10 KNET stations (Xie and Patton, 1999).

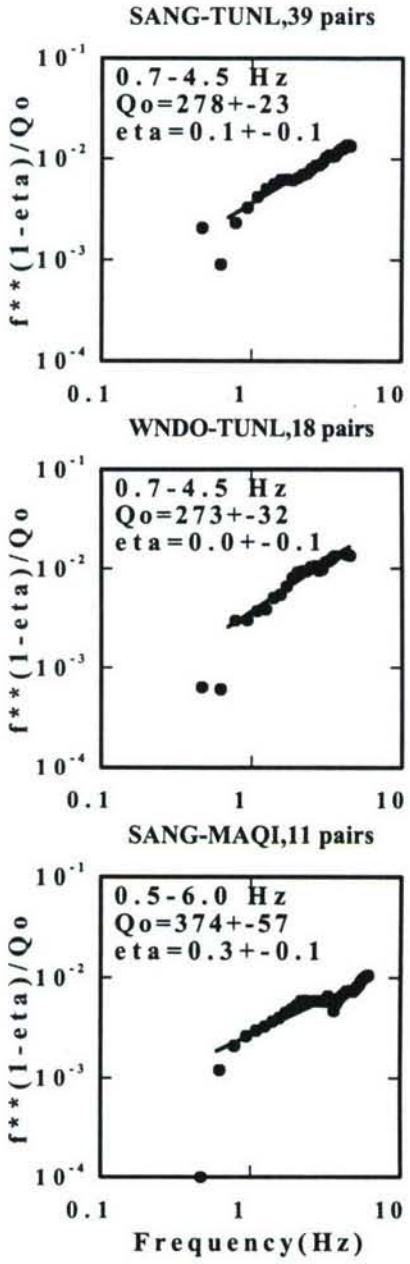

Figure 7. Stacked spectral rations (SSRs) calculated along three profiles in eastern Tibet (dots) and the best-fitting models of Q_0 and η (straight lines). Profile names and numbers of two-station pairs used are written on the top of each panel. The frequency bands used, and estimated Q_0 and η values are written inside the panels.

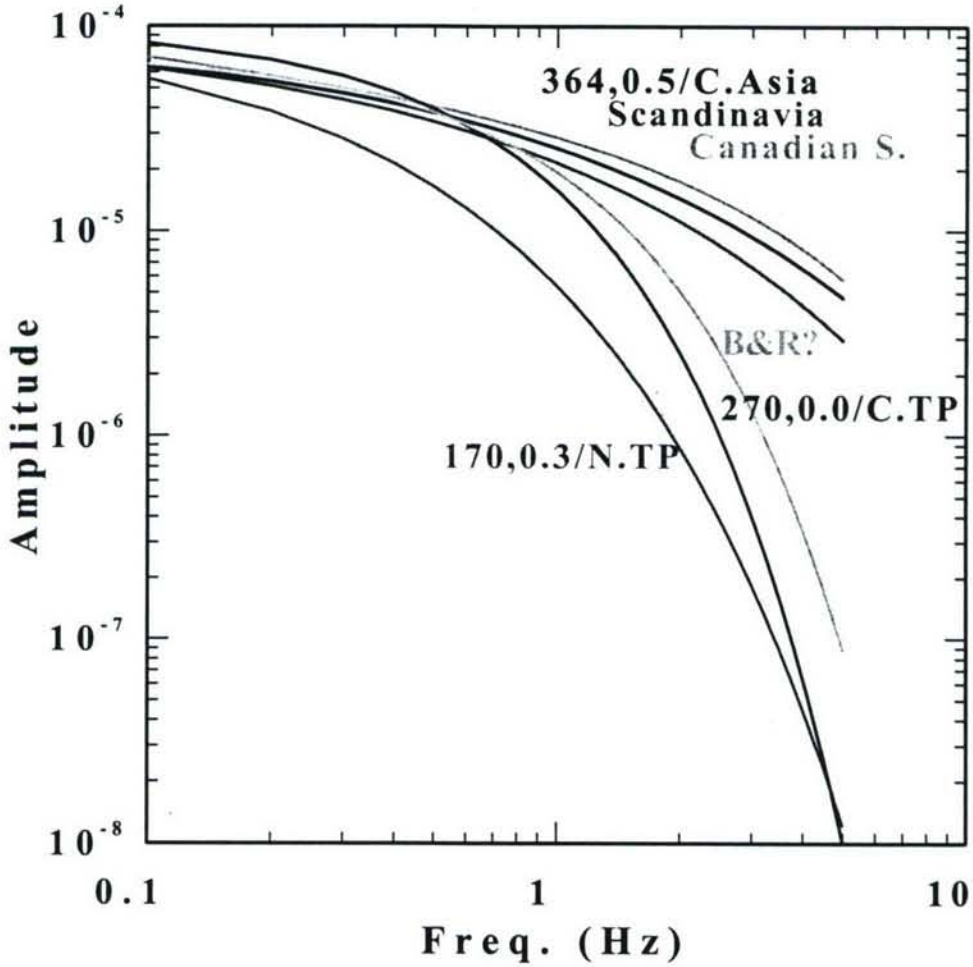

Figure 8. Pn attenuation models calculated for various regions from published literature, at a reference distance of 1200 km. Model "Canadian S." is for the Canadian shield, calculated using the Q_0 and η values and the G.S.T. by Zhu et al. (1991). Model "Scandinavia" is from Sereno et al. (1988). Model "C. Asia" is for central Asia (Xie and Patton, 1999; this study). Models "C. TP." and "N. TP." are obtained from this study for paths running from ETB to stations in south-central Tibet and north-central Tibet (gray and black paths in Figure 5), respectively. Model "B&R" is calculated by extrapolating the result of Tinker and Wallace (1997), which is obtained using Pn decay in the Basin and Range province at near-regional distances. This extrapolation is associated with an uncertainty caused by the distance evolution of Pn (see INTRODUCTION), hence the question mark. Values of Q_0 and η of the models obtained in this study are written.

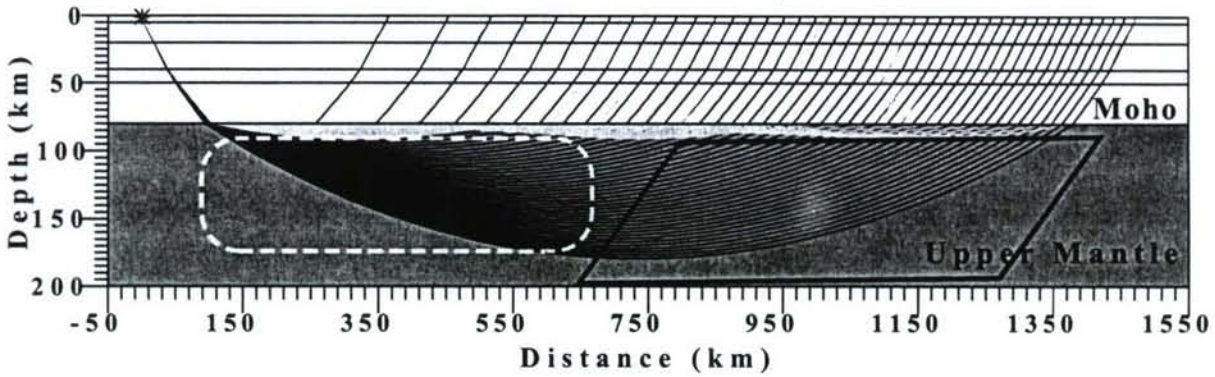

Figure 9. Pn ray patterns in a 1D velocity model constructed for Tibet using shear velocity model "S. Tibet" by Rapine et al. (2003), a Poisson ratio of 0.25, and a lid velocity gradient of 3.0 s^{-1} (Zhao and Xie, 1993). The vertical scale is exaggerated by a factor of 2. Black curves are refracted rays. Light gray curves are "whispering gallery" rays that undergo multiple (three) bounces underneath the Moho. The area delineated by the white dashed curve represents a deep-seated region with low velocity and low intrinsic Q (Q_p), such as that expected under northern Tibet. Thick black lines delineate a region with high velocity and high Q_p, expected under southern Tibet. Although the 1D structure is simplified, the ray patterns demonstrate how the refracted rays heavily sample the deep-seated anomalies. The "whispering gallery" rays, on the other hand, heavily sample structures near Moho (note the heavy concentration of light gray curves under the Moho). In the real Earth, the latter rays are expected to be also affected by 3D scatterings on or near the Moho.

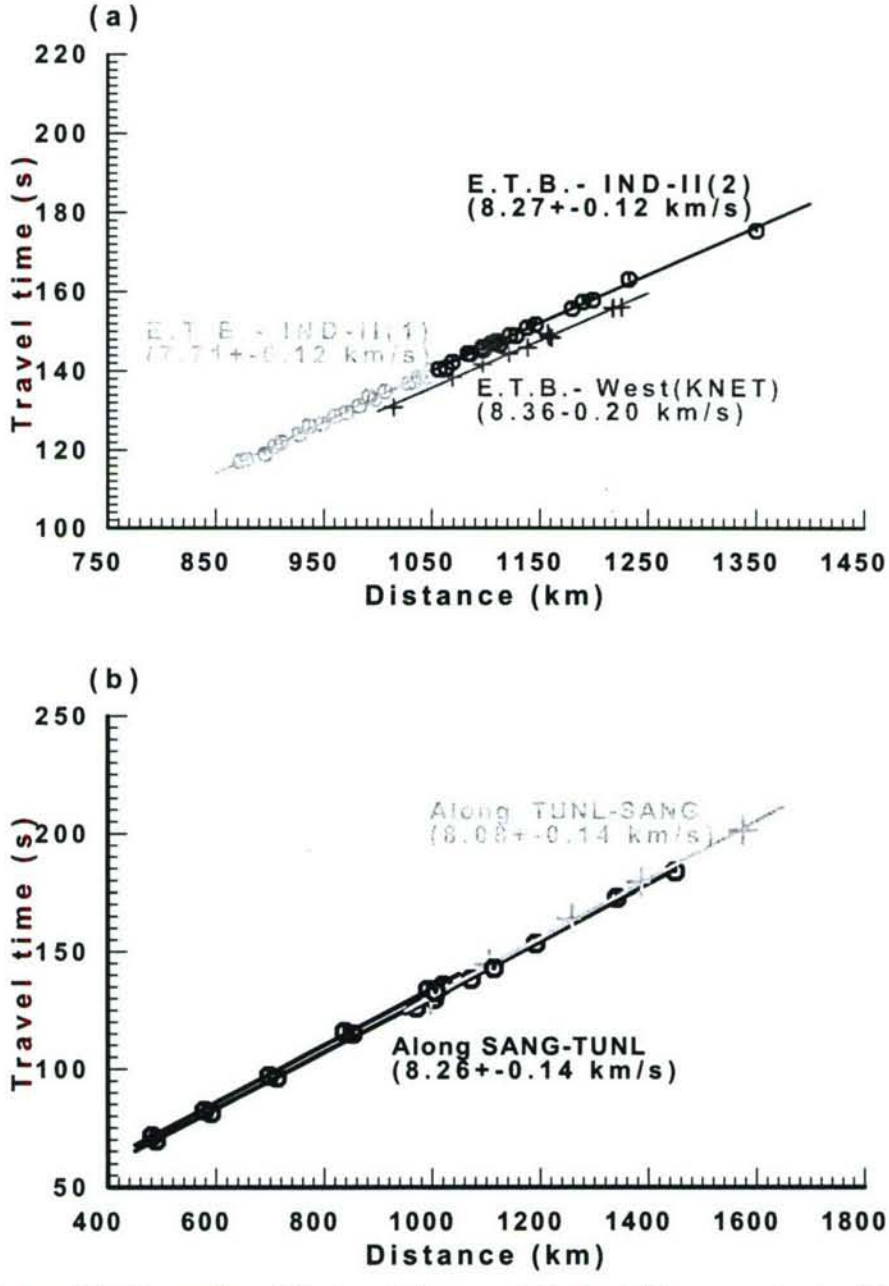

Figure 10. Exmaples of Pn travel times and the best-fit apparent velocities. Pannel (a) is for paths from earthquake 99.030 in the eastern Tarim Basin (E.T.B.) to two subgroups of INDEPTH III, and the KNET, stations. Pannel (b) is for the linear profiles delineated by stations of the 1991-1992 Tibetan Plateau experiment. Numbers in parenthes are the estimated best-fit velocities along the profiles.

Section 4

References

8301 Program Cooperation Group, 1988. Velocity structure of crust and upper mantle at the east margin of Tarim Basin and the east part of Qinghai-Tibet Plateau, in *Developments of the Research of deep Structures of China's Continent*, edited by Department of Scientific Programming and earthquake Monitoring, China Seismological Bureau, Geology Publisher, Beijing, pp 89-96.

Hearn T.M. & Clayton, R.W., 1986. Lateral velocity variations in southern-California . 2. Results for the lower crust from Pn waves, *Bull. Seism. Soc. Am*, **76**, 511-520.

Hearn, T M, Xiao, X., Ni, J.F. & the INDEPTH-III Team, 2002. Crust and Mantle Structure Beneath the INDEPTH-III Central Tibet Array, *Eos AGU Trans. 2003 Fall Meet. Suppl.* **83(47)**, F1002.

Hearn, T.M., Wang, S., Ni, J.F., Xu, Z., Yu, Y. & Zhang, X., 2004. Uppermost mantle velocities beneath China and surrounding regions *J. Geophys. Res.*, **109**, B11301, doi:10.1029/2003JB002874.

Kvaerna, T. & Doornbos, D.J., 1991. Scattering of regional Pn by Moho topography, *Geophys. Res. Lett.*, **18**, 1273-1276.

McNamara, D.T., Owens, T. & Walter, W., 1995. Observations of regional phase propagation across the Tibetan Plateau, *J. Gephys. Res.* **100**, 22,215-22,229.

McNamara, D.T., Walter, W., Owens, T. & Ammon, C., 1997. Upper mantle structure beneath the Tibetan Plateau from Pn travel time tomography, *J. Gephys. Res.* **102**, 493-505.

Menke, W. & Richards, P.G., 1980. Crust-mantle whispering gallery phases - a deterministic model of teleseismic Pn wa ve-propagation, *J. Gephys. Res.* **85**, 5416-5422.

Menke, W. & Richards, P.G., 1983. The horizontal propagation of P-waves through scattering media - analog model studi es relevant to long-range Pn propagation, *Bull. Seism. Soc. Am.*, **73**, 125-142.

Mitchell, B.J., 1995. Anelastic structure and evolution of the continental-crust and upper-mantle from seismic surface-wave attenuation *Rev. Geophys.*, **33**, 441-462.

Morozov, I.B. & Smithson, S.B., 2000. Coda of long-range arrivals from nuclear expl osions, *Bull. Seism. Soc. Am.*, **90**, 929-939.

Nelson, K.D., Zhao, W., Brown, L.D., Kuo, J., Che, J., Liu, X., Klemperer, S.L., Makovsky, Y., Meissner, R., Mechie, J., Kind, R., Wenzel, F., Ni, J., Nabelek, J., Chen, L., Tan, H., Wei, W.,

Jones, A.G. , Booker, J., Unsworth, M., Kidd, W.S.F., Hauck, M., Alsdorf, D., Ross, A., Cogan, M., Wu, C., Sandvol, E. & Edwards, M., 1996. Partially Molten Middle Crust Beneath Southern Tibet: Synthesis of Project INDEPTH Results, *Science*, **274**, 1684-1687.

Ni, J. & Barazangi, M., 1983. High-frequency seismic wave propagation beneath the Indian shield, Himalayan arc, Tibetan plateau and surrounding regions: high uppermost mantle velocities and efficient Sn propagation beneath Tibet, *Geophys. J. R. Astr. Soc*, **72**, 665-689.

Nielsen, L. & Thybo, H., 2003. The origin of teleseismic Pn waves: Multiple crustal scattering of upper mantle whispering gallery phases, *J. Geophys. Res.*, **108(B10)**, 2460, doi:10.1029/2003JB002487.

Owens T.J, Randall, G.E., Wu, F.T. & Zeng, R.S., 1993. PASSCAL Instrument performance during the Tibetan Plateau Passive Seismic experiment, *Bull. Seism. Soc. Am.*, **83**, 1959-1970.

Rapine R., Tilmann, F., West, M., Ni, J. & Rodgers, A., 2003. Crustal structure of northern and southern Tibet from surface wave dispersion ana lysis, *J. Geophys. Res.*, **108**, art. no. 2120.

Roecker, S.W., Sabitova, T.M., Vinnik, L.P., Burmakov, Y.A., Golyanov, M.I., Mamatkanova, R. & Munirova, L., 1993. Three-dimensional elastic wave structure of the western and central Tien Shan, *J. Geophys. Res.*, **98**, 15,779-15,795.

Ryberg, T., Fuchs, K., Egorkin, A.V. & Solodilov, L., 1995. Observation of high-frequency teleseismic Pn on the long-range Quartz Profile Across northern Eurasia, *J. Geophys. Res.*, **100**, 18151-18163.

Sereno, T.J., Bratt, S.R. & Bache, T.C., 1988. Simultaneous inversion of regional wave spectra for attenuation and seismic moment in Scandinavia, *J. Geophys. Res.*, **93**, 2019-2036.

Sereno, T.J. & Given, J.W., 1990. Pn attenuation for a spherically symmetric Earth model, *Geophys. Res. Lett.*, **17**, 1141-1144.

Telford, W.M., Geldart, L.P. & Sheriff, R.E., 1976. *Applied Geophysics*, Cambridge University Press, Cambridge, UK. 860 pp.

Tilmann, F., Ni, J. & the INDEPTH III Seismic Team, 2003. Seismic imaging of the downwelling Indian lithosphere beneath central Tibet, *Science*, **300(5624)**, 1424-1427.

Tinker, M.A. & Wallace, T.C., 1997. Regional phase development of the non-proliferation experiment within the western United States, *Bull. Seism. Soc. Am.*, **87**, 383-395.

Xie, J., 1996. Synthetic and observational study of Pn excitation and propagation in central Asia, *Phillips Laboratory Scientific Report No. 1*, PL-TR-96-2270, 24 pp., http://www.ldeo.columbia.edu/~xie/xie96.pdf (last accessed December, 2004).

Xie, J. & Patton, H., 1999. Regional Phase Excitation and Propagation in the Lop Nor Region of Central Asia and Implications for the Physical Basis of P/Lg Discrimi nants, *J. Geophys.*

Res., **104**, 941-954.

Xie, J., Gok, R., Ni, J. & Aoki, Y., 2004. Lateral variations of crustal seismic attenuation along the INDEPTH Profiles in Tibet from Lg Q inversion, *J. Geophys. Res.*, **109**, B10308, doi:10.1029/2004JB002988.

Zhao, X. & Ebel, J.E., 1991. Radiation pattern of crustal phases of New England earthquakes, *Geophys. J. Int.*, **106**, 647-655.

Zhao, L.S. & Xie, J., 1993. Lateral variations in compressional velocities beneath the Tibetan Plateau from Pn travel time tomography, *Geophys. J. Int.*, **115**, 1970-1084.

Zhu, T.F., Chun, K.Y. & West, G.F., 1991. Geometrical spreading and Q of Pn waves: An investigative study in eastern Canada. *Bull. Seismol. Soc. Am.*, **81**, 882-896.

Zhu, L.P. & Helmberger, D.V., 1998. Moho offset across the northern margin of the Tibetan Plateau, *Science*, **281** 1170-1172.

Appendix A

Potential Radiation Pattern from the 1999 Earthquake

In theory, Pn spectra from earthquake 99.030 may be affected by a non-isotropic source radiation pattern ($R(\theta)$ in equation (2)). In this appendix we demonstrate that the effect of this pattern is small and, when ignored, should not have caused significant errors in Pn Q estimates. First we note that this study uses finite Pn wavetrains, which are less vulnerable to the radiation pattern than are the first Pn pulses (Zhao and Ebel, 1993). To further explore the level of the radiation pattern from event 99.030, we calculate synthetic Pn wavetrains using (1) 1-D velocity model "M1" by Roecker et al. (1993), and (2) the centroid moment-tensor (CMT) solutions by Harvard and U.S. Geological Survey; both solutions characterize the source as an obliquely reverse rupture. These synthetics are then used to predict Pn radiation pattern to the directions of KNET and INDEPTH III stations (roughly west and south, respectively). The radiation predicted using the Harvard solution is about 30% higher to KNET than to INDEPTH III stations. An almost exactly opposite prediction is obtained using the USGS solution. Perturbing the 1D velocity model and focal solutions cause variations of the predictions, but the range of the variations is small, presumably because neither station group is near the Pn nodal planes. Variations in radiation pattern of such level (±30% when comparing the KNET paths to the INDEPTH paths) are less than the observed spectral variations within each station group (Figure 4). We can estimate the relative error in Pn Q_0 measurement caused by an error δx arising from an unaccounted $R(\theta)$ of 1.3, using equation (A8) of Xie et al. (2004). Assuming δx=0.3, V=7.6 km/s, f=1 Hz, and Δ=1200 km, we obtain $\delta Q_0/Q_0$ of 16% and 11% when the true Q_0 is 260 and 175, respectively. These relative errors in Q_0 are rather small and acceptable. In the true Earth structure 3D scatterings should occur to further smooth-out any radiation pattern.

Next we empirically examine whether by ignoring the effect of non-isotropic $R(\theta)$, our estimates of Q_0 and η to the INDEPTH III stations are significantly biased (see section ESTIMATES OF PN Q TO INDEPTH STATIONS). Because group III-2 of stations are located in southern Tibet and are close to the INDEPTH II stations (here after referred to as "group II"; see Figures 1 and 5), The Pn Q_0 and η from the October 7, 1994 explosion (which should not have a non-isotropic $R(\theta)$) to station group II should be similar to those from earthquake 99.030 to station group III-2. If there is a significantly non-isotropic $R(\theta)$ by event 99.030, then ignoring it should result in a biased set of Q_0 and η estimates over paths to group III-2. The bias should have masked the similarity between Q_0 and η values to group III-2 and those to group II. In the main text we ignored $R(\theta)$ and estimated average Q_0 and η values to station group III-2 to be 254±48 and 0.1±0.1, respectively. These values are close to those of 253±53 and 0.0±0.1,

paths, including the short crustal segments. Third, Pn Q may contain contributions of both intrinsic Q and scattering Q as mentioned above. In the TP, the lowest Pn Q_0, η model of 183, 0.3 is obtained for paths from ETB to northern TB. The highest Pn Q_0, η of 374, 0.3 is obtained for easternmost TP. It is possible that the former η is higher than the η of lid Q_p because of the contribution of scattering Q at higher frequencies. To explore whether temperature can provide a plausible explanation of a variation in lid Q_p under the TP, we make a simplified assumption that the η of lid Q_p in question is actually 0.2 rather than 0.3, but all the other three estimated values approximately reflect those of lid Q_p. Using equation (7) of Mitchell (1995) we estimate that, if the temperature in the mantle lid is 800°C under easternmost TB at a depths of about 150 km, then the temperature would be 1260°C under north-central Tibet. These temperatures are similar to (a) the estimates by McNamara et al. (1997) using Pn velocity variations and even more simplifications on lid Q_p, and (b) the estimates made by other authors as summarized by McNamara et al. (1997). This demonstrates that although there is much uncertainty in Q measurements and theoretical relationships, temperature variation alone can indeed explain a lateral variation in lid Q_p under the TP. A similar inference has been made about mantle shear Q in the continental U.S. by Mitchell (1995).

A by-product of this study is a set of Pn travel time measurements, which were used to estimate apparent Pn velocities under the INDEPTH and 1991-1992 TP networks. Using two-way travel times along two profiles in the eastern TB, approximate dip angles along the profiles are also estimated. The maximum dip is estimated to be 2.6° in southeast TP, indicating a crustal thinning toward north.

Appendix B

Pn Velocity Analysis

A by-product of the spectral analysis of this study is a set ot Pn arrival times, which must be read prior to the Fourier transform. These arrival times are used to estimate the apparent Pn velocity under the INDEPTH and 1991-1992 PASSCAL profiles, as well as the KNET. Figure A1 shows examples of the Pn arrival times and the best-fit apparent velocities. Table A1 summarizes the best-fit velocities along all profiles studied. As mentioned in the main text, we have divided the INDEPTH III stations into two groups that are north and south of the BNS (Figure 5; Figure A1(a)). We obtained very slow and very fast apparent velocities of 7.71±0.12 and 8.27±0.12 km/s for the northern and southern station groups, respectively. These estimates are consistent with those of Hearn et al. (2002) who used a larger set of Pn arrival times and proposed that Pn velocity changes abruptly, from about 7.7 to 8.4 km/s, across the BNS. The change is thought to be caused by hot (near solidus) mantle lid in north central Tibet, and cold lid in the south (see INTRODUCTION).

Along the 1991-1992 profiles (SANG-TUNL and SANG-MAQI) two-way arrival times are available, yielding average apparent Pn velocities that are more reliable estimates of the true lid velocity when the Moho dips (Telford et al., 1976; equation (4.54a)). We estimated that the average apparent velocity can vary from the one-way apparent velocities by about 0.1 km/s (Figure A1). Along profiles SANG-TUNL and SANG-MAQI, the estimated two-way average Pn velocity are 8.1 to 8.3 km/s (Table A1), indicating an eastward increase of lid velocity. This is consistent with the eastward increase of Pn Q_0 reported in the main text. The average dipping angles along these two profiles are also estimated using equation (4.53) of Telford et al. (1976), and listed in Table A1.

DISTRIBUTION LIST
DTRA – TR – 05 – 30

DEPARTMENT OF DEFENSE

DEFENSE TECHNICAL INFORMATION CENTER
8725 JOHN J. KINGMAN ROAD, SUITE 0944
FT. BELVOIR, VA 22060-6201
2 CYS ATTN: DTIC/OCA

DEFENSE THREAT REDUCTION AGENCY
8725 JOHN J. KINGMAN ROAD STOP 6201
FT. BELVOIR, VA 22060-6218
2 CYS ATTN: RD-NTX/E. STOKES

DEPARTMENT OF DEFENSE CONTRACTORS

ITT INDUSTRIES
ITT SYSTEMS CORPORATION
1680 TEXAS STREET, SE
KIRTLAND AFB, NM 87117-5669
2 CYS ATTN: DTRIAC
ATTN: DARE

LAMONT-DOHERTY EARTH OBSERVATORY
OF COLUMBIA UNIVERSITY
61 ROUTE 9W
PALISADES, NY 10964
ATTN: JIAKANG XIE